Chemical synthesis of nonstoichiometric NiO$_x$ nanoparticles using different nickel salts and application as an additive or interface layer in photovoltaic devices

Fatma Pınar CHOI[*]

Department of Physics, Faculty of Arts and Science, Yıldız Technical University, İstanbul, Turkey

Abstract: The stoichiometric nickel oxide is an insulator while it becomes a p-type semiconductor with the presence of divalent and trivalent states. Here nonstoichiometric nickel oxide nanoparticles (NiO$_x$ NPs) were synthesized via a chemical route using two different starter salts; nickel chloride hexahydrate and nickel nitrate hexahydrate. The nanoparticles were investigated by X-ray diffraction and transmission electron microscopy, scanning electron microscopy, to determine the crystal structure, morphology, and particle size. The effect of different nickel salts in the reaction and the formation of NiO$_x$ nanoparticles were observed for the first time in the literature. Because of the high uniformity and stability, nitrate-based inks were employed as additives and interface layers for planar perovskite solar cells, using a two-step deposition for regular (n-i-p) and one-step antisolvent washing method for inverted (p-i-n) configurations. Photovoltaic performances were improved in the case of NiO$_x$ applied as an interface layer between P3HT and Ag for regular solar cells and both as an additive in sol-gel based NiO$_x$ and interface layer between HTL and perovskite in inverted solar cells.

Key words: Nanoparticle synthesis, chemical precipitation, nonstoichiometric nickel oxide, nickel chloride hexahydrate, nickel nitrate hexahydrate, solar cells

1. Introduction

The importance of nanotechnology and nanomaterials cannot be ignored with day by day extending application areas for several industries. Nanomaterials are defined with dimensions up to 100 nm and may exhibit completely different fascinating features compared to their bulk and molecular counterparts. This potential induced a worldwide raising interest in the investigation of nanomaterials for environmental, medical-pharmaceutical, energy-related, catalytical, cosmetical, electronical, magnetical, optical, and many other fields [1]. Metal oxide-based nanomaterials particularly crystalline ones gained a lot of attention owing to their broad diversity, novel physicochemical characteristics originating from the limited size/density of surface sites, stability, and facile posttreatment free employment. Numerous methods were developed for the synthesis of these materials based on two main transformations such as gas to solid and liquid to solid [2]. Gas to solid routes including various types of chemical vapor deposition [3] and pulsed laser depositions [4] provide ultrafine particle synthesis with high uniformity and reproducibility. Liquid to solid routes are favoured due to easy control of morphology including chemical coprecipitation [5], sol-gel [6], solvothermal [7], microemulsion [8], and surface template [9] methods. Simplicity, cost/product efficiency, toxicity, and reproducibility very important for these processes.

---

[*]Correspondence: gokdemir@yildiz.edu.tr

Wet methods are widely favoured since they are simple, cost-effective, and easy to control. The surface template method employs surfactants or porous solids as soft or hard templates for mediating self-assembled nanoparticle systems, respectively. In the microemulsion (direct inverse micelles) method, a mixture of surfactant, an aqueous metal solution, and oil used for precipitation of metal precursor in an oxo-hydroxide form with a limited size by oxo-hydroxide-surfactant contact. The solvothermal method based on the decomposition of metal complexes utilizes pressure by an autoclave or boiling in an inert system with an agent surfactant. This agent is expected to control particle shape, size, and undesired agglomeration. Sol-gel is another frequently used route that engages the steps of hydrolysis, polycondensation, drying, and calcination. Normally, alcoholic precursors of alkoxides employed and hydrolysis result in a metal hydroxide network. The resulted network of hydroxyl-species builds a dense porous gel by condensation and nanoparticles achieved after drying and calcination processes. For metal oxide nanosized materials chemical precipitation method is the most cost-effective, easy, and does not require high laboratory conditions. In this route, chloride or nitrate-based metal salt's aqueous precursor used as a starter and a base solution handled for precipitation of oxo-hydroxide by controlling anion and cations. However, particle size, shape, and homogeneity controlling is relatively challenging and may require the help of other surfactants, sonochemical processes. Here the calcination temperature is a key point for complete decomposition and particle size that affects the basic characteristics of the material including, structural (surface geometry, crystal planes and lattice), electronic (quantum size confinement, bandgap) thus physical and chemical (conductivity, reactivity) [10–13]. Among these metal oxides, nickel oxide is an environment-friendly candidate with high stability. It is known as an insulator in the stoichiometric form it turns into a p-type semiconductor in nonstoichiometric form. NiO_x with a wide bandgap between 3.6–4.0 eV, and a conduction band level around 1.8 eV and unique structural [14], electrical, optical, and magnetic properties enable its adoption as hole conducting material for solar cells in other words a p-type transparent conductor [15], a cathode for lithium-ion batteries [16], an anode for solid oxide fuel cells [17], gas sensors [18], anodic colouring layer for electrochromic devices [19], catalysts [20], and antiferromagnetic coatings [21]. This study gives a detailed report on the synthesis of nanocrystalline NiO_x powders based on the chemical precipitation method using two different nickel salts. Effect of starter salt on the produced NiO_x particle size, solubility, stability, optical and structural properties were investigated through, XRD, SEM, TEM, Uv-Vis spectrophotometry. Nitrate-based salt employed powder was found to exhibit better size uniformity with lower grains, higher solubility, stability, and thereby it was employed as an interface layer and/or additive for improving the hole transport in regular and inverted type planar perovskite solar cells.
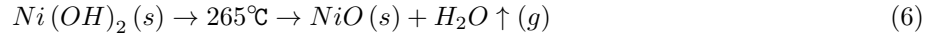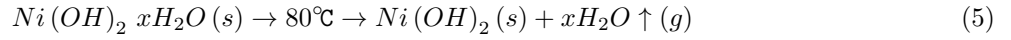
2. Materials and methods
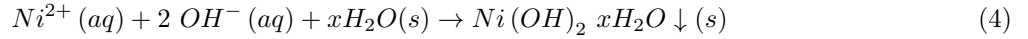
2.1. Materials
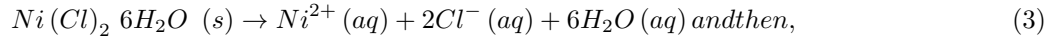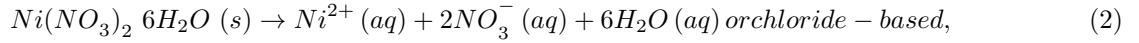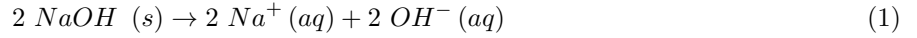
Materials employed in nanoparticle synthesis and solar cell fabrication are including, nickel (II) chloride hexahydrate ($NiCl_2$ $6H_2O$, >99.9%, Aldrich), nickel (II) nitrate hexahydrate ($Ni(NO_3)_2$ $6H_2O$, > 99.9%, Aldrich), sodium hydroxide (NaOH, ACS reagent, ≥97.0%, pellets, Sigma-Aldrich Corp., St. Louis, MO, USA), nickel (II) acetate tetrahydrate ($Ni(OCOCH_3)_2$ $4H_2O$, > 99.0%, Aldrich), MEA (ethanolamine purified by redistillation, 99.5%, Sigma-Aldrich Corp.), lead iodide (PbI_2, 99.0%, Sigma-Aldrich Corp.), MAI (CH_3NH_3I, 99.99%, Lumtec, Luminescence Technology Corp., Taipei City, Taiwan), PCBM ([6,6]-phenyl-C61-butyric acid methyl ester, 99.95%, nano-C), BCP (2,9-dimethyl-4,7-diphenyl-1,10-phenanthroline, 96%, Sigma Technologies S.L., Madrid, Spain), poly(3-hexylthiophene-2,5-diyl) (P3HT, >99.9%, Sigma-Aldrich Corp.), titanium(IV) isopropoxide ($Ti[OCH(CH_3)_2]_4$, ≥97.0%, Sigma-Aldrich Corp.), acetylacetone ($CH_3COCH_2COCH_3$, Reagent

Plus, $\geq$ 99%, Sigma-Aldrich Corp.), gamma-butyrolactone (GBL, $C_4H_6O_2$, Reagent Plus, $\geq$99% Sigma-Aldrich Corp.), toluene ($C_6H_5CH_3$, EMPLURA Merck-Millipore, Merck KGaA, Darmstadt, Germany), ITO-coated glass substrates (35–45 Ω/sq, Kintec Global Recruitment Ltd., Manchester, UK) were purchased and used without additional purification.

2.2. Chemical precipitation based synthesis of the NiO_x nanoparticles

Nonstoichiometric nanoparticles of nickel oxide were obtained using a chemical precipitation method [5,15]. Two different nickel salts such as nickel (II) chloride hexahydrate and nickel (II) nitrate hexahydrate were employed to compare the nanoparticle qualities. Figure 1 displays the synthesis steps for black powders.

The reactions were givenas follows:

$$2\ NaOH\ (s) \rightarrow 2\ Na^+\ (aq) + 2\ OH^-\ (aq) \tag{1}$$

$$Ni(NO_3)_2\ 6H_2O\ (s) \rightarrow Ni^{2+}\ (aq) + 2NO_3^-\ (aq) + 6H_2O\ (aq)\ or\ chloride-based, \tag{2}$$

$$Ni\ (Cl)_2\ 6H_2O\ (s) \rightarrow Ni^{2+}\ (aq) + 2Cl^-\ (aq) + 6H_2O\ (aq)\ and\ then, \tag{3}$$

$$Ni^{2+}\ (aq) + 2\ OH^-\ (aq) + xH_2O(s) \rightarrow Ni\ (OH)_2\ xH_2O \downarrow (s) \tag{4}$$

$$Ni\ (OH)_2\ xH_2O\ (s) \rightarrow 80\text{℃} \rightarrow Ni\ (OH)_2\ (s) + xH_2O \uparrow (g) \tag{5}$$

$$Ni\ (OH)_2\ (s) \rightarrow 265\text{℃} \rightarrow NiO\ (s) + H_2O \uparrow (g) \tag{6}$$

First, 0.5 M nickel salt (nickel chloride hexahydrate and nickel nitrate hexahydrate) was dissolved in water at room temperature for 15 min and resulted in a clear green solution. 10 N sodium hydroxide solution prepared by dissolving NaOH pellets in deionized water. 10 N NaOH solution was drop by drop introduced to the aqueous Ni precursor till the pH became 10 and the colloidal precipitation of white-green $Ni(OH)_2$ was completed. Obtained turbid solution was washed with water by sonication and centrifuged at 5000 rpm for 7 min. This step was repeated at least 3 times. Subsequently, a filtering system with a hydrophilic PVDF 0.2 μm paper filter was used to take paste-like green products. This product was dried in a vacuum oven overnight at 80 °C and then hand-milled by a ceramic mortar prior to the calcination. Finally, light green fine powder of $Ni(OH)_2$ was annealed in an air furnace at 265 °C for 2 h, and black powder of NiO_x was obtained by decomposition of $Ni(OH)_2$ to NiO_x and water.

3. Preparation of the coating precursors

3.0.1. Preparation of nanoinks

Synthesized NiO_x NPs were found to be dispersible in various solvents such as deionized water, n-butanol, 2-methoxy ethanol, methanol, isopropanol. Since the perovskite layer is profoundly influenced by water, isopropanol was chosen as the solvent. 30 mg of NiO_x NPs mixed with 1 mL isopropanol and mixed in an ultrasonic bath at 50 °C for at least 6 h and filtered by 0.45 μm PVDF syringe filters to obtain the nanoinks. NiO_x NPs were used in two different ways; first, nanoinks were directly coated on sol-gel deposited NiO_x HTLs
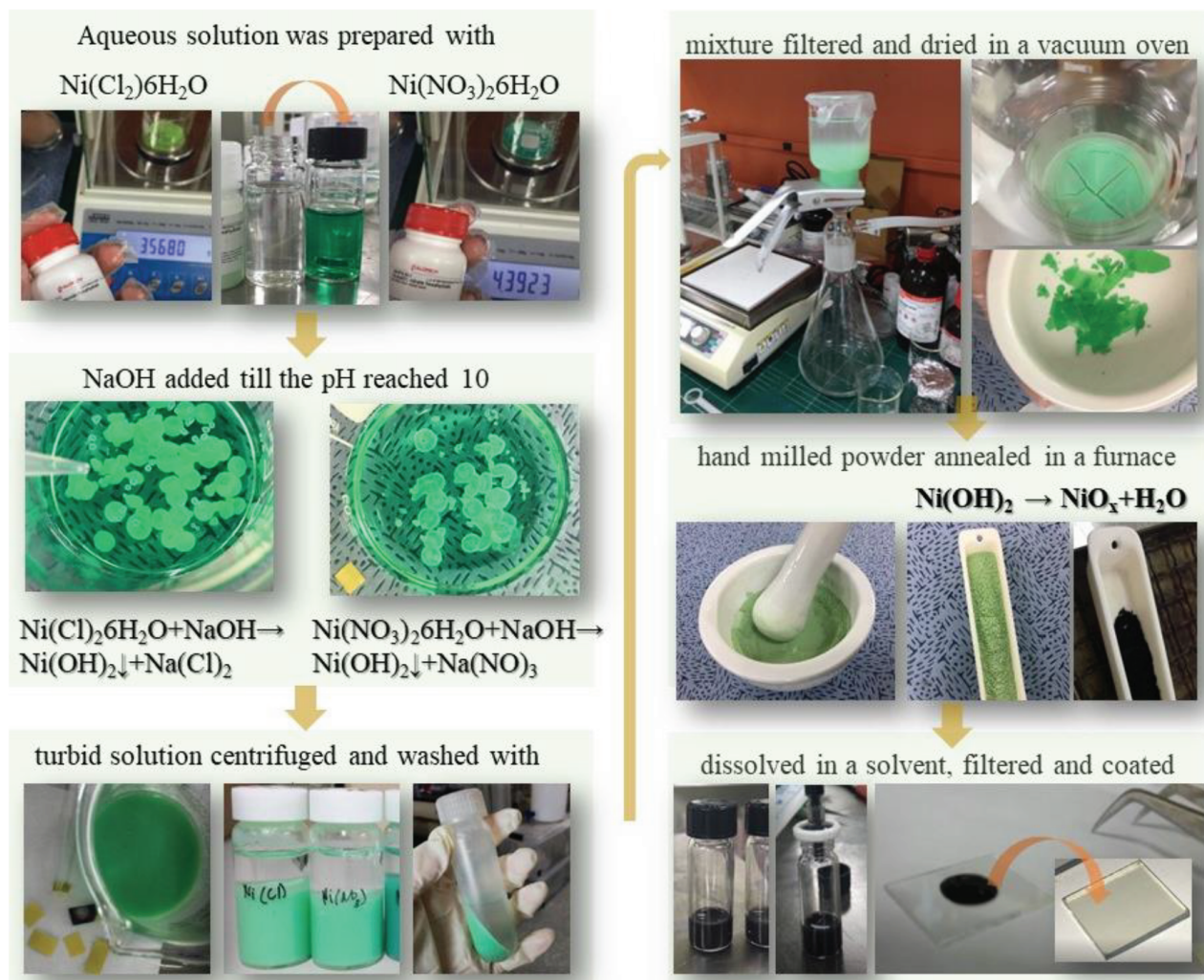
Figure 1. NiO$_x$ nanoparticle synthesis steps.

for p-i-n-type solar cells and labeled as NiO$_x$ / NiO$_x$ NP. Similarly, they were coated on P3HT HTLs for n-i-p-type solar cells and were labeled as P3HT/ NiO$_x$ NP. Second; 30 mg/mL of NiO$_x$ NPs dissolved in NiO$_x$ sol-gel precursor and P3HT precursor and was labeled as NiO$_x$: NiO$_x$ NP and P3HT: NiO$_x$ NP, respectively.

3.0.2. Preparation of hole transporter precursors

P3HT based HTL was simply prepared by dissolving 10 mg of P3HT powder in chlorobenzene and stirring at 45–50 °C for 2 h. This clear dark orange solution was used without any filtering. NiO$_x$ HTL precursor was prepared by admixing 1.244 g of nickel (II) acetate tetrahydrate in 50 mL isopropanol at room temperature for 15 min on a magnetic stirrer. However, complete dissolution of nickel salt was not possible then 300 µL of MEA was introduced into this green mixture as a coordinating agent. With the addition of MEA, the colour of the green solution turned to blue. Later, the glass vial was sealed with Teflon tape for heating treatment up to 75–80 °C on a magnetic stirrer and in 15 min colour of the mixture changed to green by the complete

dissolution of nickel salt. Yet, the solution stirred at 75–80 °C for 4 h and was used in 48 h. Before the coating step, solution was filtered by a 0.22 µm PTFE filter.

3.0.3. Preparation of electron transporter precursors

PCBM ETL precursor was simply obtained by dissolving 20 mg of PCBM powder in chlorobenzene at 45–55 °C for at least 6 h. TiO_2 ETL precursor was prepared by mixing 1.4 mL of titanium (IV) isopropoxide with 1 mL of acetylacetone. Since the reaction is exothermic acetylacetone was kept cold and magnetically stirred in an ice bath for 30 min. The resulted transparent stock solution was in a yellow-orange colour and diluted (1:10 by weight) by the addition of ethanol drop by drop during stirring. Before the coating step solution was filtered by a 0.22 µm PTFE filter.

3.0.4. Preparation of perovskite layer precursors

Perovskite fabrications were used as GBL based one-step for inverted solar cells and a 2-step method for regular solar cells. One-step perovskite precursor was prepared by dissolving 3.87 g PbI_2 and 1.33 g MAI in 6 ml GBL at 70 °C for at least 12 h. Before the coating step, the warm solution was double filtered by a 0.22 µm PTFE filter. The solution was kept at 70 °C during coating. For 2-step fabrication; there were two different precursors. First; PbI_2 precursor was obtained by mixing 1 M PbI_2 in DMF: DMSO (7:3 by volume) at 70 °C for 4 h. The solution was kept at 60 °C during coating. Second, MAI precursor was obtained by dissolving 5 g MAI in 100 mL isopropanol at 40 °C for 2 h. The solution was kept at room temperature during coating.

4. Thin film and device preparation

All the glass-based substrates were ultrasonically cleaned in acetone and warm isopropanol at 65 °C for 30 min each. Thin-film layers of NiO_x nanoinks (30 mg/mL) were deposited at 3000 rpm for 30 s and dried on a hot plate at 90 °C for 90 s used for optical measurements. For inverted type solar cell fabrication; NiO_x solution was spin-coated on clean ITO coated glasses (1.5 cm × 1.5 cm) at 1500 rpm for 30 s and dried at 80 °C for 20 min on a hot plate. Then for the second layer spin coating was repeated by NiO_x solution or NiO_x NPs including NiO_x solution. These layers were annealed in a furnace at 450 °C for 1 h. For NiO_x/ NiO_x NPs configuration 30 mg/mL NiO_x nanoink spin-coated onto NiO_x sol-gel deposited layers at 3000 rpm for 30 s and dried at 90 °C for 90 s. HTL coated substrates kept at 90 °C on a hot plate and GBL based perovskite precursor (at 70 °C) spin-coated at 2000 rpm 10 s and 4000 rpm 20 s. After 3 s of the second step 60 µL toluene was dropped on the center of the spinning substrates. After the toluene washing colour was changed to dark brown indicating the perovskite formation. Then substrates subsequently transferred on to a hot plate at 100 °C that was checked by IR-thermometer and annealed for 10 min for complete crystallization. Without waiting annealed perovskite layers were covered by PCBM solution and cast at 2500 rpm for 35 s. PCBM coated layers were dried at 90 °C for 90 s and then BCP solution spin-coated at 2000 rpm for 40 s. For regular type solar cell fabrication; TiO_2 ETL layers were deposited onto ITO coated glass substrates by spin coating TiO_2 precursor at 8000 rpm for 30 s at room temperature. TiO_2 coated layers were annealed in an air furnace at 450 °C for 1 h. After cooling down toroom temperature (RT) a thin layer of PCBM (10 mg/mL) was cast at 4000 rpm 30 s and dried at 90 °C for 90 s. Perovskite layer fabrication started with the PbI_2 layer deposition, warm PbI_2 precursor spin-coated on TiO_2/PCBM coated substrates at 2000 rpm 45 s and annealed on a hot plate at 150 °C for 20 min. Homogenous yellow PbI_2 layers were obtained and after cooling down to the RT, MAI

precursor(at RT) dropped on to these layers, waited for 7 s, and cast at 5000 rpm for 30 s. Right after the dropping of the MAI precursor, the colour of the PbI_2 layer was changed to brownish and turned completely dark brown after transferring to the hot plate that was kept at 100 °C for 10 min. Without waiting and as fast as possible, P3HT layer or NiO_x NPs including the P3HT layer was spin-coated on perovskite layers at 2500 rpm for 30 s and dried on a hot plate at 90 °C for 90 s. For P3HT/ NiO_x NPs substrates NiO_x nanoink cast at 3000 rpm for 30 s and dried on a hot plate at 90 °C for 90 s. Solar cell device fabrications were completed by the thermal evaporation of a 100-nm thick Ag metal contacts. Except for the metal contact evaporation, including perovskite layer formation all steps were carried in ambient air under a moderate level of humidity around 50%–55 %.

5. Characterizations

The crystal structure, surface morphology, shape, and sizes of the nanoparticles were analyzed by X-ray diffractometer (Rigaku Ultima IV, Applied Rikagu Technologies, Inc., Austin, TX, USA), field emission scanning electron microscope (Hitachi S-4300, Hitachi, Ltd., Tokyo, Japan), and transmission electron microscope (JEOL JEM 2010, JEOL Ltd., Tokyo, Japan). The optical absorbance of the nanoinks and transmittance of the nanoink coated glass substrates were collected by a UV-Vis spectrophotometer (Shimadzu UV-1601PC, Shimadzu Corp., Kyoto, Japan). Nanoink employed regular and inverted type solar cells were examined by a Keithley 2400 model current-voltage measuring unit (Tektronix UK Ltd., Bracknell, UK) that connected with an ABET model solar simulator (Abet Technologies Inc., Milford, CT, USA). Current-voltage data recorded in a glove-box, under 100 mW/cm^2 illumination, AM 1.5G with 0.25 V/s scan rate, and 0.03 s delay time.

6. Results

NiO_x nanoink and XRD patterns of the NiO_x NPs that were prepared by nickel nitrate hexahydrate and nickel chloride hexahydrate were depicted in Figures 2a and 2b. First, it should be noted that the resulted NPs were identical in a dark black powder form. Even though nanoinks were also similar after first preparation in IPA, chloride-based NPs tend to precipitate faster than nitrate-based ones, Figure 2a. The reason behind this difference might be originating from different formation of NPs under the same calcination process. Because the air annealing temperature is a key point for the decomposition of $Ni(OH)_2$ powders into the NiO_x and temperatures below 270 °C may result in remaining $Ni(OH)_2$ species which are related to lower electrical conductivity of NiO_x NPs and its dispersibility in the solvent. However, higher temperatures will also provoke increased particle size and then aggregation problems [5,13]. In our case for both NiO_x NPs, XRD patterns confirmed $Ni(OH)_2$-free formation of cubic NiO_x phase (JCPDS 22-1189) and a noticeable size difference with widened peak widths for nitrate-based powder. Diffraction peaks for the (111), (200), and (220) planes were placed at similar degrees [22] and given in Table 1. Crystallite sizes "D" were calculated using Debye–Scherrer equation [23];

$$D = 0.89 \ \lambda/\beta cos\theta, \tag{7}$$

where 0.89, β, θ, and λ are the correction factor, FWHM of the related peak (radian), diffraction angle and the wavelength of the employed X-ray (0.154 nm), respectively. Calculated crystalline sizes were found to be larger for the chloride-based starters used NPs. Moreover, "d" spacing values and "a" lattice constants extracted from XRD data using the following equations.

$$2dsin\theta = n\lambda \ , \tag{8}$$

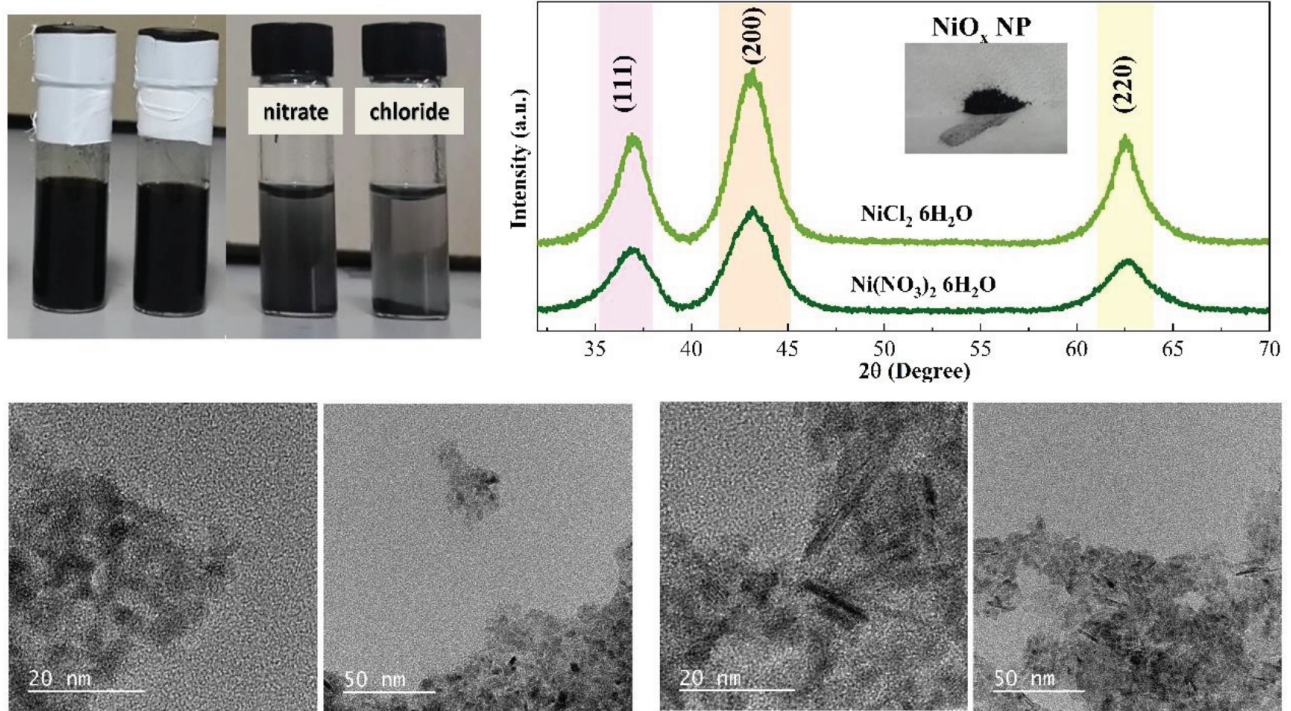$$a_{cubic} = d\sqrt{h^2 + k^2 + l^2}. \tag{9}$$

Figure 2. (a) NiO$_x$ nanoinks (for 1 week), (b) XRD patterns of NiO$_x$ nanopowder, TEM images of NiO$_x$ nanopowder synthesized by (c) nickel nitrate hexahydrate, (d) nickel chloride hexahydrate.

Table 1. Crystallographic data for NiO$_x$ nanopowder.

Nanopowder	hkl plane	2θ (°)	D (nm)	d (Å)	a (Å)
Chloride-based	111	36.97	4.38	2.429	4.207
	200	43.07	3.79	2.098	4.196
	220	62.51	3.92	1.484	4.197
Nitrate-based	111	37.02	3.13	2.425	4.200
	200	43.18	3.04	2.093	4.186
	220	62.61	2.70	1.482	4.192

TEM images for the nitrate and chloride-based starters used NPs were shown in Figures 2c and 2d, respectively. TEM images indicated a better uniformity with particle sizes lower than 5 nm for nitrate-based NPs which is compatible with the XRD results. Also, slightly larger and different shape formations such as needle-like particles with over 10 nm were existing together with the regular shaped nanoparticles observed for the chloride-based NPs. Figures 3a and 3b display the EDS (energy dispersive spectroscopy) results for NPs and curves exhibited the Ni-O peaks with an atomic ratio of 39.12–47.4 and 49.77–43.82 for chloride and nitrate-based NPs, respectively. Here, some impurities such as Cl, Na, and C were also observed with a higher atomic ratio in the case of chloride-based NPs. Also increased O/Ni ratio in the case of chloride-based NPs suggests the

rod-like shape formations as reported by Song et al. [24]. UV-Vis spectrophotometry was used to investigate the optical band gap and transmittance of the nanoinks and NiO_x NP layers deposited on glass substrates were given in Figures 4a and 4b, respectively. Absorbance spectra of the nanoinks around 375–385 nm correspond to the optical bandgap absorption with a slight blue shift for nitrate-based nanoinks, as expected. Transmittance curves (Figure 4b) for NiO_x NP layers on glass substrates showed high transparency in the visible range between 85%—90% for both layers regardless of nickel salt which is desired for the full utilization of the solar spectrum. Tauc plots extracted from transmittance data using Tauc formula;

$$(\alpha h\upsilon)^n = A\left(h\upsilon - E_g\right), \tag{10}$$

where "a" is absorption coefficient calculated using transmittance data as "–1/d ln(T)" and, "hν" is the photon energy, "A" and "n" constants where n is 2 for a direct allowed transition. Thus optical gap can be estimated from the extrapolation of the linear part of the Tauc plot where α goes to zero [25]. As mentioned, depicted optical band gaps were around 3.59 and 3.63 eV for chloride and nitrate-based NiO_x NP, respectively. Increased optical band gap values for nitrate-based nanoink coated layers also indicated a decrease in particle size which is a well-known phenomenon for semiconductor nanoparticles [26]. Even though optical properties of the nitrate and chloride-based nanoparticles are comparable, because of the ink stability and shape uniformity of nitrate-based nanoinks used for further applications. Figure 5 shows the optical microscopy and various type SEM images of nitrate-based NiO_x NP layers deposited on perovskite at 3000 rpm 30 s. From the crosssectional image, a 75 nm of NP film (green) thickness was observed on the perovskite layer (brown), Figure 5d. Since the NP film thickness measured as 75 nm, nanoparticles were also noticeable from the crosssectional view as estimated from the TEM and XRD results. Further, the applicability of NP layers in photovoltaic devices was investigated through perovskite methylammonium lead tri-iodide ($CH_3NH_3PbI_3$) based solar cells that is a popular absorber that energetically fits with NiO_x and takes attention in inverted (p-i-n) [27,28] and regular (n-i-p) [29] type solar cells. As mentioned in the experimental part, perovskite layer formation was carried out by 2 different routes such as "one-step" and "two-step" for inverted (ITO/NiO_x NP modified NiO_x sol-gel/$CH_3NH_3PbI_3$/PCBM/BCP/Ag) and regular (ITO/TiO_2(sol-gel)/PCBM/$CH_3NH_3PbI_3$/NiO_x NP modified P3HT/Ag) configurations as shown in Figure 6, respectively. Solar cell parameters extracted from the J-V curves were given in Table 2. Except for the regular type where P3HT is used as an HTL, the contribution of NiO_x NPs displayed a beneficial effect for each case. In other words when NiO_x NPs were employed as an additive or interface layer only the additive form of NiO_x NPs in P3HT resulted in degradation. This degradation might be linked to the overdose doping of the P3HT solution. Moreover, P3HT employed regular cells exhibited low performance as expected, yet provided a comparison. Lower FF values were associated with the high resistivity of ITO coated glass substrate and humidity level during perovskite formation. For regular structure when NiO_x NPs were employed as an interface layer between HTL and metal contact, open circuit voltage (V_{OC}), short circuit current density (J_{SC}) thus power conversion efficiency (PCE) increased in a percentage of 12.9%, 8%, and 10.6%, respectively. Increased V_{OC}, values are thought to be related to the enhanced energy alignment between perovskite and the NiO_x NPs modified HTL [30]. Highest occupied molecular orbital (HOMO) and lowest unoccupied molecular orbital (LUMO) levels of the P3HT are known to be around 5.0 and 3.0 eV, respectively. For NiO_x, its valance band and conduction band are reported to be around 5.2 and 1.8 eV, respectively. Hence, better hole transportability of the NiO_x HTLs with the electron blocking property of the NiO_x NP layer is thought to induce a decreased recombination and leakage currents. This might be correlated with the increased short circuit current densities in the NiO_x NP modified devices.
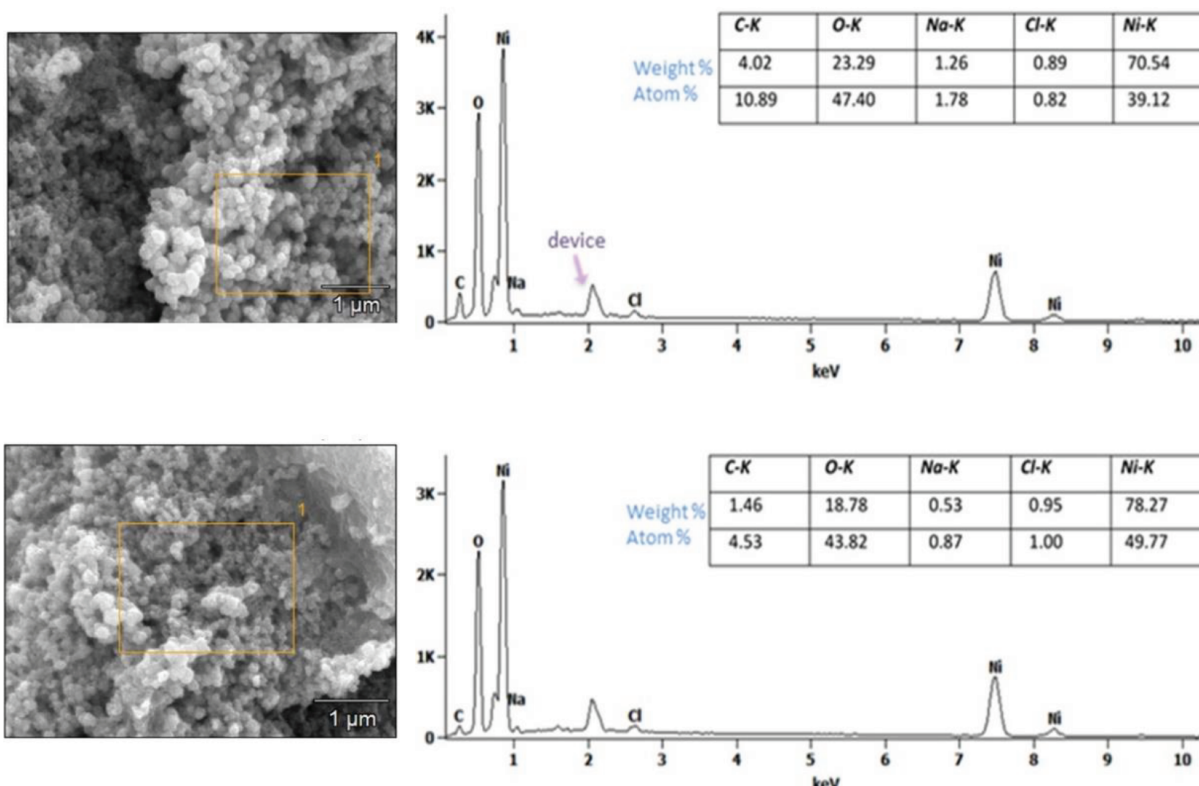
Figure 3. SEM images and EDS spectra of NiO$_x$ nanoparticle synthesized by (a) nickel chloride hexahydrate, (b) nickel nitrate hexahydrate.
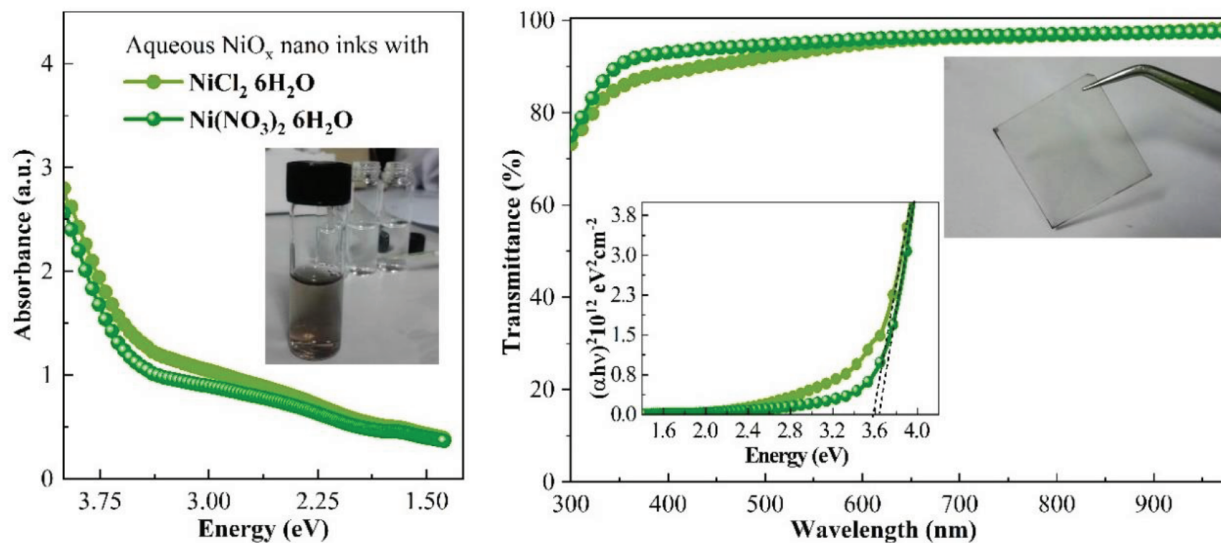

Figure 4. (a) Absorbance spectra of nanoinks (10 μL of 30 mg/mL filtered nanoink, in 1 mL IPA), (b) transmittance spectra and Tauc plots of NiO$_x$ nanoparticle films coated on glass substrates at 3000 rpm for 30 s.
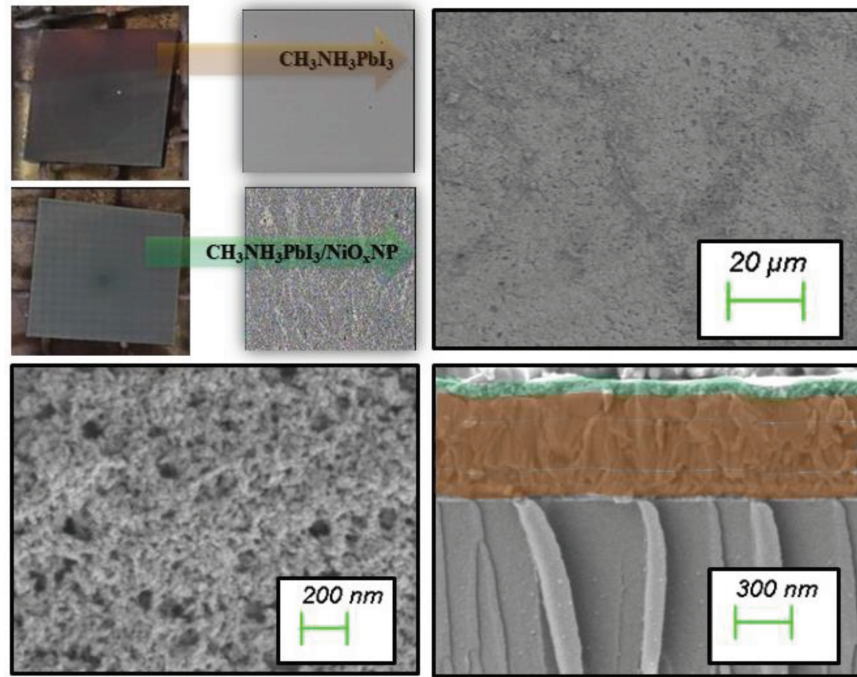
Figure 5. (a) Photograph and optic microscope images of perovskite and NiO$_x$ nanoparticle coated perovskite layers, SEM images of nickel (II) nitrate hexahydrate based NiO$_x$ nanoparticle films deposited on perovskite layers for (b) 700 X, (c) 50 KX magnifications and, (d) crosssectional with 40 KX magnification.
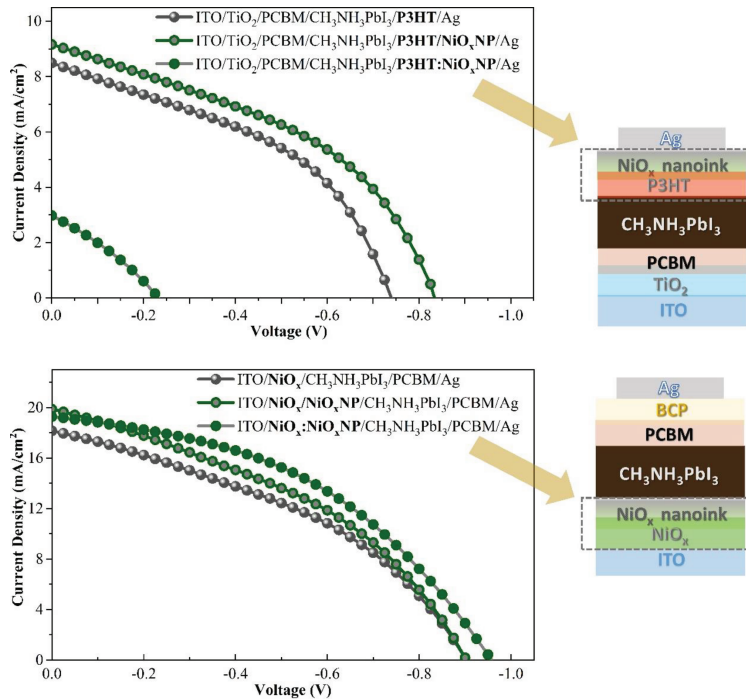

Figure 6. Current density-voltage curves for NiO$_x$ nanoparticle employed (a) regular and (b) inverted type solar cells with corresponding device schemes.

Table 2. Photovoltaic parameters for NiO_x nanoparticle employed solar cells.

HTL structure	J_{SC} $(mAcm^{-2})$	V_{OC} (mV)	FF	PCE (%)
P3HT	8.52	739	0.42	2.84
P3HT/NP	9.19	834	0.41	3.14
P3HT:NP	3.02	229	0.34	2.35
NiO_x	18.1	902	0.40	6.53
NiO_x/NP	19.9	902	0.53	9.51
NiO_x:NP	19.3	958	0.44	8.14

For inverted type cells, NiO_x NP modification resulted in increased FF, V_{OC}, and J_{SC} values for both. As an additive it boosted V_{OC}, FF, J_{SC} thus PCE with a percentage of 6.2%,10%, 6.6%, and 24.7%, respectively. When it was used as an interface layer between HTL and perovskite layer,V_{OC}, FF, J_{SC} thus PCE values were increased with a percentage of 6.2%, 32.5%, 9.9%, and 45.6%, respectively. It is known that the NiO_x powders exhibit more favorable outcomes compared to the sol-gel based NiO_x layers [31], such as better crystallinity, higher conductivity, and superior energy alignment with slightly higher work function values. Besides, the lower surface coverage of NiO_x powders is still a challenge and might result in less homogenous surfaces with higher RMS values when the NiO_x NP layers were employed alone. As a result, charge transport properties might be affected in an undesired way. In this work, NiO_x NP modified HTL employed devices exhibited better performances by increasing short circuit densities and fill factor values compared to the reference cells. While open circuit voltage is increased up to the highest value in the case of NiO_x powders used as an additive, decreased fill factors of these devices resulted in lower power conversion efficiencies contrasted to the interface layer employed devices.

7. Conclusion

NiO_x nanoparticles with particle sizes between 3–5 nm, were synthesized using a chemical precipitation method reacting aqueous nitrate and chloride-based nickel salt precursors with sodium hydroxide. X-ray diffraction patterns of the resulted NiO_x nanopowders corresponded to the cubic nonstoichiometric NiO_x. Compared to the nickel chloride hexahydrate, TEM images revealed that nickel nitrate hexahydrate used NiO_x nanoparticles resulted in more uniform particle shapes with lowered sizes additionally improved stability. Larger particle sizes and generation of rod-like shapes confirmed with optical and energy dispersive to spectroscopy, respectively. Owing to better stability which designates the better dispersibility in the solvent, nitrate-based nanoparticles employed in inverted and regular type solar cells as an additive or interface layer. Except for being an additive in P3HT hole transport material, NiO_x nanoparticles improved the photovoltaic performance of the devices.

References

[1] Baker GA. Nanoparticles: From Theory to Application Edited by Günter Schmid (University of Duisberg-Essen). Weinheim, Germany: Wiley-VCH Verlag GmbH & Co. KGaA, 2004.

[2] Buzby S, Franklin S, Shah SI. Synthesis of metal-oxide nanoparticles: gas-solid transformations. In: Synthesis, Properties and Applications of Oxide Nanoparticles. Hoboken, NJ, USA: John Wiley & Sons, Inc., 2007.

[3] Nakaso K, Han B, Ahn KH, Choi M, Okuyama K. Synthesis of non-agglomerated nanoparticles by an electro-spray assisted chemical vapor deposition (ES-CVD) method. Journal of Aerosol Science 2003; 34 7: 869-881. doi: 10.1016/S0021-85020300053-3

[4] Zhang J, Chaker M, Ma D. Pulsed laser ablation based synthesis of colloidal metal nanoparticles for catalytic applications. Journal of Colloid and Interface Science 2017; 1 489: 138-149. doi: 10.1016/j.jcis.2016.07.050

[5] Jiang F, Choy WC, Li X, Zhang D, Cheng J. Post-treatment-free solution-processed non-stoichiometric NiOx nanoparticles for efficient hole-transport layers of organic optoelectronic devices. Advanced Materials 2015; 27 18: 2930-2937. doi: 10.1002/adma.201405391

[6] Danial AS, Saleh MM, Salih SA, Awad MI. On the synthesis of nickel oxide nanoparticles by sol-gel technique and its electrocatalytic oxidation of glucose. Journal of Power Sources 2015; 20 293: 101-108. doi: 10.1016/j.jpowsour.2015.05.024

[7] Yin X, Liu J, Ma J, Zhang C, Chen P et al. Solvothermal derived crystalline NiOx nanoparticles for high performance perovskite solar cells. Journal of Power Sources 2016; 15 329: 398-405. doi: 10.1016/j.jpowsour.2016.08.102

[8] Han DY, Yang HY, Shen CB, Zhou X, Wang FH. Synthesis and size control of NiO nanoparticles by water-in-oil microemulsion. Powder Technology 2004; 147 (1-3): 113-116. doi: 10.1016/j.powtec.2004.09.024

[9] Wang TJ, Huang H, Wu XR, Yao HC, Li FM et al. Self-template synthesis of defect-rich NiO nanotubes as efficient electrocatalysts for methanol oxidation reaction. Nanoscale 2019;11 42: 19783-19790. doi: 10.1039/C9NR06304H

[10] Sheena PA, Priyanka KP, Sabu B, Varghese T. Effect of calcination temperature on the structural and optical properties of nickel oxide nanoparticles. Nanosystems: Physics, Chemistry, Mathematics 2014; 5 3: 441-449.

[11] Bahari Molla Mahaleh Y, Sadrnezhaad SK, Hosseini D. NiO nanoparticles synthesis by chemical precipitation and effect of applied surfactant on distribution of particle size. Journal of Nanomaterials 2008; 2008: 470595. doi: 10.1155/2008/470595

[12] Khoshhesab ZM, Sarfaraz M. Preparation and characterization of NiO nanoparticles by chemical precipitation method. Synthesis and Reactivity in Inorganic, Metal-Organic, and Nano-Metal Chemistry 2010; 40 9: 700-703. doi: 10.1080/15533174.2010.509710

[13] Yin X, Chen P, Que M, Xing Y, Que W et al. Highly Efficient flexible perovskite solar cells using solution-derived NiOx hole contacts. ACS Nano 2016; 10 3: 3630-3636. doi: 10.1021/acsnano.5b08135

14 Sato H, Minami T, Takata S, Yamada T. Transparent conducting p-type NiO thin films prepared by magnetron sputtering. Thin Solid Films 1993; 236 (1-2): 27-31. doi: 10.1016/0040-60909390636-4

[14] Zhang H, Cheng J, Lin F, He H, Mao J et al. Pinhole-free and surface-nanostructured NiOx film by room-temperature solution process for high-performance flexible perovskite solar cells with good stability and reproducibility. ACS Nano 2016; 10 1: 1503-1511. doi: 10.1021/acsnano.5b07043

[15] Rai AK, Anh LT, Park CJ, Kim J. Electrochemical study of NiO nanoparticles electrode for application in rechargeable lithium-ion batteries. Ceramics International 2013;39 6: 6611-6618. doi: 10.1016/j.ceramint.2013.01.097

[16] Lu Y, Gasper P, Pal UB, Gopalan S, Basu SN. Improving intermediate temperature performance of Ni-YSZ cermet anodes for solid oxide fuel cells by liquid infiltration of nickel nanoparticles. Journal of Power Sources 2018; 396: 257-264. doi: 10.1016/j.jpowsour.2018.06.027

[17] Mokoena TP, Swart HC, Motaung DE. A review on recent progress of p-type nickel oxide based gas sensors: future perspectives. Journal of Alloys and Compounds 2019; 15 805: 267-294. doi: 10.1016/j.jallcom.2019.06.329

[18] Sun DL, Zhao BW, Liu JB, Wang H, Yan H. Application of nickel oxide nanoparticles in electrochromic materials. Ionics 2017; 23 6: 1509-1515. doi: 10.1007/s11581-017-1974-4

[19] Fominykh K, Feckl JM, Sicklinger J, Döblinger M, Böcklein S et al. Ultrasmall dispersible crystalline nickel oxide nanoparticles as high-performance catalysts for electrochemical water splitting. Advanced Functional Materials 2014; 24 21: 3123-3129. doi: 10.1002/adfm.201303600

[20] Tadic M, Nikolic D, Panjan M, Blake GR. Magnetic properties of NiO (nickel oxide) nanoparticles: blocking temperature and Neel temperature. Journal of Alloys and Compounds 2015; 25 647: 1061-1068. doi: 10.1016/j.jallcom.2015.06.027

[21] Beach ER, Shqau K, Brown SE, Rozeveld SJ, Morris PA. Solvothermal synthesis of crystalline nickel oxide nanoparticles. Materials Chemistry and Physics 2009;115 1: 371-377. doi: 10.1016/j.matchemphys.2008.12.018

[22] Birks L. Friedman H. Particle size determination from X-ray line broadening. Journal of Applied Physics 1946; 17: 687-692. doi: 10.1063/1.1707771

[23] Song X, Gao L. Facile synthesis and hierarchical assembly of hollow nickel oxide architectures bearing enhanced photocatalytic properties. The Journal of Physical Chemistry C 2008;112 39: 15299-15305. doi: 10.1021/jp804921g

[24] Tauc J, Menth A. States in the gap. Journal of Non-crystalline Solids. 1972; 1 8: 569-585. doi: 10.1016/0022-30937290194-9

[25] Moriarty P. Nanostructured materials. Reports on Progress in Physics 2001; 64 3: 297. doi: 10.1088/0034-4885/64/3/201

[26] Choi FP, Alishah HM, Bozar S, Doyranli C, Koyuncu S et al. A novel interface layer for inverted perovskite solar cells fabricated in ambient air under high humidity conditions. Solar Energy 2020; 1 209: 400-407. doi: 10.1016/j.solener.2020.08.013

[27] Shin GS, Choi WG, Na S, Gökdemir FP, Moon T. Lead acetate based hybrid perovskite through hot casting for planar heterojunction solar cells. Electronic Materials Letters 2018; 14 2: 155-160. doi: 10.1007/s13391-018-0042-1

[28] Choi WG, Kang DW, Na S, Park CG, Gokdemir FP et al. Sequentially vapor-grown hybrid perovskite for planar heterojunction solar cells. Nanoscale Research Letters 2018; 13 1:1-6. doi: 10.1186/s11671-017-2401-5

[29] Ye M, He C, Iocozzia J, Liu X, Cui X et al. Recent advances in interfacial engineering of perovskite solar cells. Journal of Physics D: Applied Physics 2017; 50 37: 373002. doi: 10.1088/1361-6463/aa7cb0

[30] Seo YH, Cho IH, Na SI. Investigation of sol-gel and nanoparticle-based NiOx hole transporting layer for high-performance planar perovskite solar cells. Journal of Alloys and Compounds 2019; 797: 1018-1024. doi: 10.1016/j.jallcom.2019.05.204